Electron Beam Effects on AES Depth Profiling of SiO_2 Thin Film on Si(001): a Factor Analysis Study

Daisuke Fujita [a,*], Keiko Onishi [a], Taro Yakabe [a] and Kazuhiro Yoshihara [b]
[a] *National Institute for Materials Science, 1-2-1 Sengen, Tsukuba 305-0047, Japan*
[b] *ULVAC-PHI, Inc., 370 Enzo, Chigasaki, Kanagawa, 253-8522, Japan*
*fujita.daisuke@nims.go.jp

(Received: August 16, 2006 ; Accepted: August 30, 2006)

Electron beam irradiation effects on the Auger depth profiling with Ar^+ ion-beam sputtering on a SiO_2 thin film formed on Si(001) has been studied using target factor analysis (TFA). TFA depth profiling has proved itself a powerful tool for chemical state analysis of the overlapped Auger peaks originated from SiO_2 and elemental Si. Especially, the existence of sub-stoichiometric oxide with oxygen-deficient centers at the SiO_2/Si(001) interface has been clarified. Significant influence of electron beam irradiation on depth profiling has been demonstrated at the beam densities in excess of ~0.5 A/cm^2. Further increase of the electron beam density leads to the enhancement of the sputtering rate and the deterioration of the depth resolution. The observed enhancement in the sputtering rate is attributed to the electron-beam induced desorption of oxygen from the topmost surface region of SiO_2, which creates the less stable sub-stoichiometric SiO_x layer containing oxygen-deficient center defects. Since the SiO_2 thin films on Si(001) substrates are widely used for the calibration of depth scale, careful optimization of beam density is required for quantitative depth profiling.

1. Introduction

Dielectric oxide thin films, such as silicon dioxide (SiO_2) thin films formed on Si(001) substrates, are key materials for metal-oxide-semiconductor field-effect transistors (MOSFET) and have been widely used for engineering applications [1]. The surface chemical compositions of such dielectric thin films are often evaluated by surface chemical analysis techniques [2, 3]. Especially for the surface mapping and in-depth distribution analysis of chemical composition of thin film, Auger electron spectroscopy (AES) combined with a scanning electron microbeam source and a focused ion sputtering apparatus using inert gas have been widely used [4]. Since AES has a superior surface sensitivity of a few nanometer range and an excellent lateral resolution of a submicron scale, it will be a powerful tool for a surface chemical analysis of microelectronics applications.

However, increased electron beam current density with an enhancement of spatial resolution may cause a significant damage to oxide thin films. Especially for silicon dioxides, it is recognized that a focused electron beam may partially dissociate SiO_2 [5, 6]. Dissociation of SiO_2 can be observed mainly as a significant change of Si LVV peak shape, from the oxide state to an elemental-like state [5]. Such electron beam dissociation can be used for a direct mask-less patterning at sub-micron scale [7]. Using a sharp tip of scanning tunneling microscopy (STM) as a field-emitted electron source, direct nanoscale lithography has been demonstrated on SiO_2/Si(001) substrates [8]. Mechanism of electron-beam induced dissociation can be qualitatively understood as electron stimulated desorption (ESD) of oxygen from the oxides and subsequent formation of oxygen-deficient defects or sub-oxides (SiO_x) in SiO_2 [9-11].

On the other hand, SiO_2 thin films formed on Si(001) substrates have been widely used for routine calibration of the depth scale for AES depth profiling analysis, where AES spectra are measured sequentially as a function of sputtering time [12]. For quantitative depth profiling, it is required to convert the sputtering time scale to the sputtered depth scale. Therefore, it is important to clarify any possible electron-beam effects on the sputter etching of the reference materials for depth calibration. In the case of SiO_2 thin films formed by thermal oxidation, significant enhancement of the effective sputter-etching rate caused by electron beam irradiation has been reported [10,13].

In this article, we investigate on the effects of electron-beam current density on the depth profiling of sputter-deposited SiO_2 thin film on Si(001) in detail by means of target factor analysis [14-16]. Compared to conventional treatment of Auger data, more information can be obtained in this way [17]. AES depth profiling analysis can be performed either by discontinuously after subsequent sputtering steps or by continuous sputtering and simultaneous electron spectros-

Copyright (c) 2006 by The Surface Analysis Society of Japan

copy. Here we adopted the former case. Thus the effect of damage from the electron beam irradiation on the sputter-etching rate and depth profiling property such as depth resolution has been studied especially.

2. Experimental

2.1 Sample and Measurements

The sample is a SiO_2 thin film formed on a Si(001) substrate by magnetron sputtering deposition. The thickness of the film is 104 nm. The Auger depth profiling was performed at room temperature within a scanning Auger microprobe facility (PHI, SAM 660). The analysis chamber was fitted with a differentially pumped ion gun for specimen cleaning and depth profiling. The base pressure in the analysis chamber was $\sim 1 \times 10^{-8}$ Pa. The heart of the system is a cylindrical mirror analyzer (CMA) with a coaxially mounted electron gun with a LaB_6 cathode. The relative energy resolution ($\Delta E/E$) of the CMA was set to 0.6 %, where E represents kinetic energy of emitted electrons. The angle of incidence of the electron beam was 30 degrees from the sample surface normal. The primary energy and incidence current of the electron beam were 10 keV and 1.69 µA, respectively. To observe the influence of electron beam density on depth profiling, the current density of the incidence beam were changed from 0.081 A/cm^2 to 4.7 A/cm^2 by changing the raster-scanned area. For comparison, the point-analysis mode of approximately ~200 A/cm^2 was also used. For the depth profiling, sputtering was performed by rastering a focused 1.4 keV Ar^+ ion beam over an area of 2 mm × 2 mm. The depth profiles resulted from the repetition of ~100 cycles, each made of the Ar^+ sputtering for 12 s followed by Auger spectra acquisition. Data were acquired in steps of 0.5 eV over three energy regions of 50-100 eV, 492-520 eV and 1592-1622 eV, corresponding to Si LVV, O KLL and Si KLL line shapes, respectively. The electron irradiation doses during a single step of sputter-etching were ranging from 2.5 to ~6200 C/cm^2 depending on the electron current densities. The minimum dose of 2.5 C/cm^2 corresponds to the reported value of critical electron dose for 1% decomposition of SiO_2 thin film [11].

2.2 Target Factor Analysis

Target factor analysis (TFA) is a multivariate technique for reducing matrices of data to their lowest dimensionality and can extract physically meaningful factors by using a target transformation [18]. TFA can be applied to the case where the data can be modeled as a linear sum of product terms as shown below.

$$D_{ij} = \sum_{k}^{n} R_{ik} C_{kj} \tag{1}$$

Here spectrum intensity $D_{i,j}$ at energy i of sample j can be represented by a linear sum of concentration C_{kj} of species k in sample j and its standard spectrum intensity R_{ik} at energy i in 100% concentration. The number of terms in the sum, n, is called the number of factors. Since TFA employs the whole information included in the spectra rather than the conventional peak-to-peak or peak-to-background intensity measurements where most of the data information is not used efficiently, more reliable and informative analysis may become possible. Especially TFA is a very powerful tool when the energy regions of interested species are overlapped. In such cases, quantitative peak intensity measurements are very difficult by the conventional methods. Here, our interest is on the change of chemical states during depth profiling from the dioxide state (SiO_2) to elemental Si one, where the interested line shapes are mostly overlapped. Therefore, data sets of the Auger depth profiling measurements were processed by TFA.

The data treatment procedure for a set of data composed of c spectra (samples) in the depth profile and r energy points in each spectrum is shown in Fig. 1. At first a sequence of $EN(E)$ spectra obtained during the Auger depth profiling are stored in a single data file. Since the noise and background should be reduced sufficiently, the raw data are smoothed and differentiated by using the Savitzky-Golay algorithm for smoothing and differentiation [19], and saved as a data matrix $\boldsymbol{D}$. Since the column vectors of the experimental data matrix $\boldsymbol{D}$ are composed of the treated differential $dEN(E)/dE$ spectra, the matrix size of $\boldsymbol{D}$ is $r \times c$. Then the covariance matrix Z is constructed by pre-multiplying the data matrix $\boldsymbol{D}$ by its transpose $\boldsymbol{D}^{\mathrm{T}}$. This $c \times c$ covariance matrix is diagonalized by the Jacobi eigenanalysis method [20], yielding eigenvalues matrix $\boldsymbol{\lambda}$ and eigenvector matrix $\boldsymbol{Q}$. The diagonal elements of the eigenvalues matrix $\boldsymbol{\lambda}$ are eigenvalues λ_i sorted by the magnitude order ($\lambda_1 > \lambda_2 > \ldots > \lambda_c$). Each column vector of the eigenvector matrix $\boldsymbol{Q}$ is the eigenvector of corresponding eigenvalue. At this stage the factor space is c dimensions since all of the factors originating from experimental errors are included. The correct number of factors, n, can be determined by various ways [18]. Once the number of factors is determined correctly, the matrices, $\boldsymbol{\lambda}$ and $\boldsymbol{Q}$, are reduced to n dimensions matrices, $\boldsymbol{\lambda}^+$ and $\boldsymbol{Q}^+$, which are further transformed to abstract row and column matrices, $\boldsymbol{R}^+$ and $\boldsymbol{C}^+$, as shown below.

$$\boldsymbol{C}^+ = \boldsymbol{Q}^+, \quad \boldsymbol{R}^+ = \boldsymbol{D}\boldsymbol{Q}^+ \tag{2}$$

Here the data matrix can be reproduced by the abstract row and column matrices as below.

$$\boldsymbol{D} = \boldsymbol{R}^+ \boldsymbol{C}^+ \tag{3}$$

In order to give the physical meanings to the abstract matrices, it is required to find out the transformation matrix $\boldsymbol{T}$ to transform the factor space, which can be performed by tar-

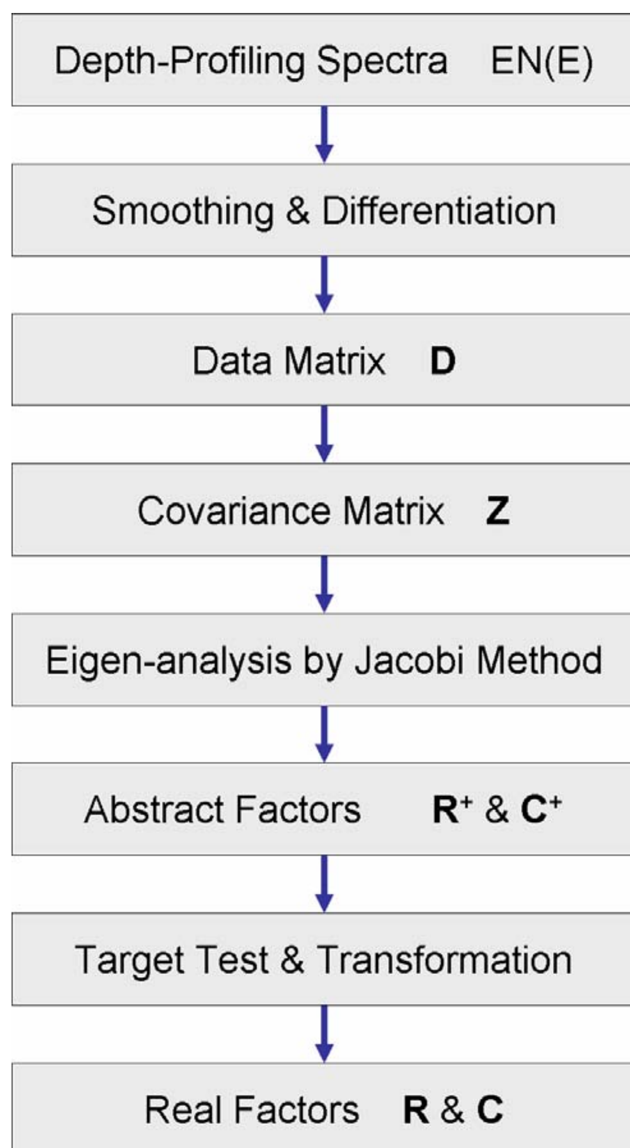

Fig. 1 The data treatment procedure for the depth profiling spectra using target factor analysis.

get transformation involving target testing. The test vectors called *targets* for the target testing are selected, which are suspected to be basic factors. The transformation matrix $\boldsymbol{T}$ can be obtained by least-squares procedure to minimize the deviation between the test vectors and the corresponding predicted vectors. By applying $\boldsymbol{T}$ and $\boldsymbol{T}^{-1}$ to the abstract matrices, the physically meaningful factors, $\boldsymbol{R}$ and $\boldsymbol{C}$, can be extracted as below.

$$\boldsymbol{D} = (\boldsymbol{R}^{+}\boldsymbol{T})(\boldsymbol{T}^{-1}\boldsymbol{C}^{+}) = \boldsymbol{RC} \tag{4}$$

Here $\boldsymbol{C}$ is composed of the column factors corresponding to the sequential change of concentration during depth profiling.

3. Results

Figure 2 (a)-(d) show the sequential changes of line shape in Si $L_{2,3}VV$ (hereafter LVV) Auger spectra for different electron beam current densities during the depth profiling of the SiO_2 thin film on Si(001). In the case of relatively lower current density as shown in Fig. 2 (a), it is possible to see an abrupt change of line shape from SiO_2 to elemental Si. The line shapes and peak positions of SiO_2 (73 eV) and elemental Si (90 eV) in *EN(E)* mode are in good accordance with the previous reports [9,17]. On the contrary, with increasing current density, it is possible to observe the additional peak at around 87 eV in *EN(E)* line shape, which can be attributed to the initial formation of oxygen-deficient center (ODC), located at 3 eV below the elemental Si peak [9]. At the highest current density as shown in Fig. 2 (d), the continuous growth of the ODC peak was observed and the interface between SiO_2 and elemental Si became ambiguous.

Figure 3 (a)–(d) show sequential changes of line shape in Si KL_3L_3 (hereafter KLL) Auger spectra for different electron beam current densities during the depth profiling of the SiO_2 thin film on Si(001). It should be noted that the energy resolution ΔE at this high energy range is approximately 10 eV, much more degraded than that (~0.5 eV) of low energy range as shown in Fig. 2. As for the relatively lower current density cases as shown in Fig. 3 (a) and (b), it is possible to recognize line shapes corresponding to SiO_2 and elemental Si. The Si KLL peak positions of SiO_2 (1603 eV) and elemental Si (1613 eV) in *EN(E)* mode show a relatively good accordance with the previously reported values [3, 21,22]. On the contrary, in the cases of higher current densities as shown in Fig. 3 (c) and (d), the gradual growth of the shoulder peak at around 1611 eV was observed in the oxide region which can be attributed to a sign of ODC formation. Consequently the interface between SiO_2 and elemental Si became obscure.

Figure 4 (a)-(d) indicate sequential changes of O KLL Auger spectra during the depth profiling of the SiO_2 thin film on a Si(001) substrate. The O KLL peak position of SiO_2 regions was observed at 502 eV in *EN(E)* mode showing a good accordance with the previously reported value [3]. Slight peak shift to higher energy (503 eV) was observed at the interface, which may be attributed to the existence of sub-stoichiometric silicon oxide. With increasing the current density of primary beam, the transition between SiO_2 and background became more and more vague.

Figure 5 shows the typical example of data pre-treatment process of Auger depth profiling spectra of Si LVV for TFA in the case of low current density. The sequential set of raw spectra was numerically smoothed by using Savitzky-Golay smoothing as shown in Fig. 5 (b) where the background fluctuation was still remained. The Auger spectra after the subsequent Savitzky-Golay differentiation shown in Fig. 5 (c) clearly indicate that the background fluctuation is significantly reduced. The data sets of differentiated Auger spectra were used for TFA.

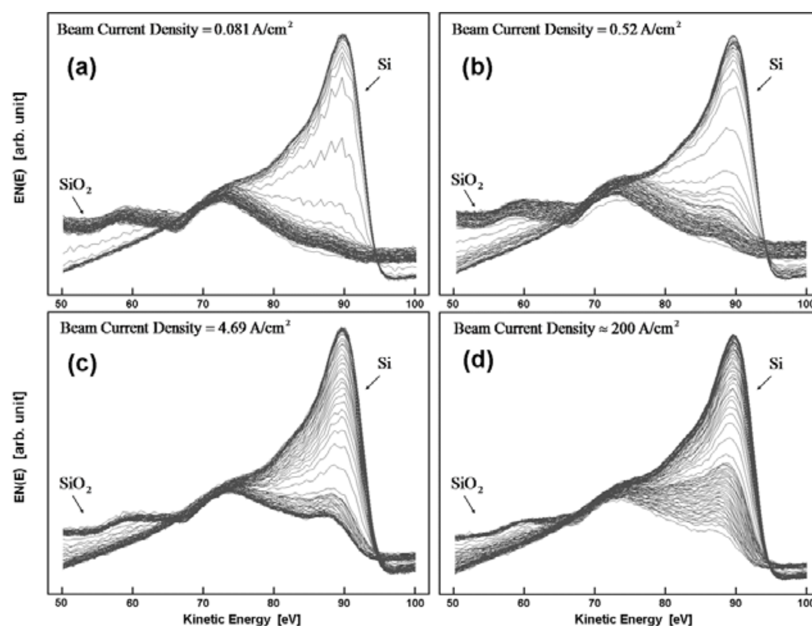

Fig. 2 Sequential changes of Si LVV Auger spectra during the depth profiling of the SiO_2 thin film (104 nm) on a Si(001) substrate.

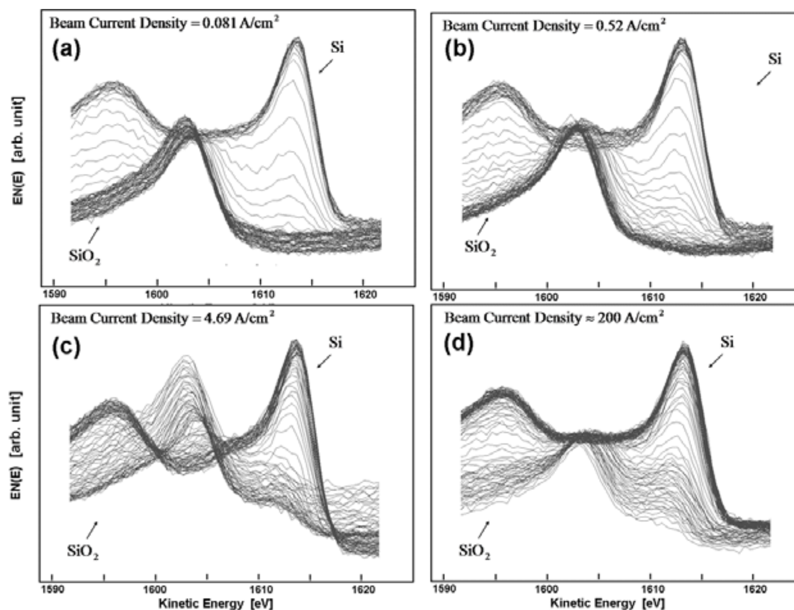

Fig. 3 Sequential changes of Si KLL Auger spectra during the depth profiling of the SiO_2 thin film (104 nm) on a Si(001) substrate.

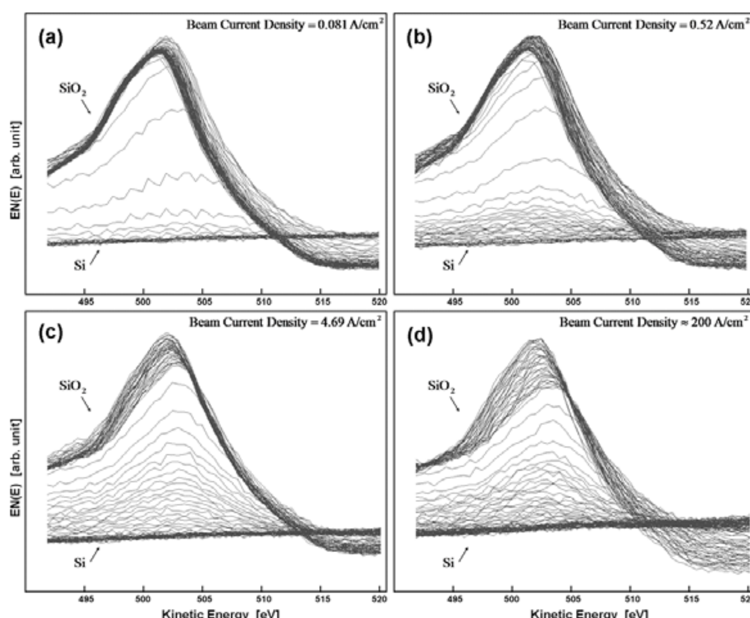

Fig. 4 Sequential changes of O KLL Auger spectra during the depth profiling of the SiO_2 thin film (104 nm) on a Si(001) substrate.

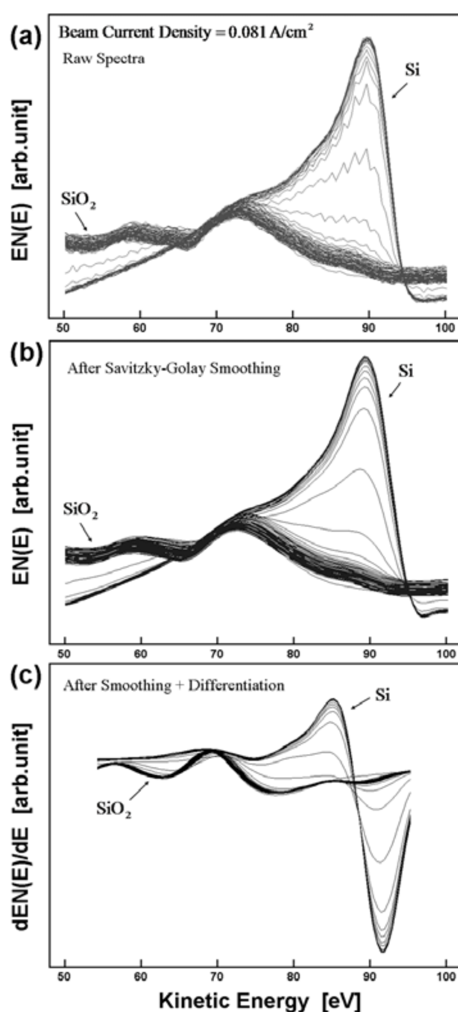

Fig. 5 Data pre-treatments of Auger spectra for the target factor analysis in the case of a relatively lower current density of 0.081 A/cm^2. (a) Raw Si LVV spectra. (b) The Auger spectra after Savitzky-Golay smoothing. (c) The Auger spectra after subsequent Savitzky-Golay differentiation.

4. Discussion

4.1 Depth Profiling of SiO_2/Si Interface

At first the detailed analysis on the depth profile of SiO_2/ Si(001) interface is considered in the case of a relatively low current density of primary electron beam. Figure 6 shows the depth profile of SiO_2/Si(001) interface observed with an electron beam current density of 0.081 A/cm^2. There are various criteria for deducing the exact size of the true factor space [18]. Among them we used the variance defined as below.

$$\textit{Variance} = \frac{\lambda_j}{\sum_{j=1}^{c} \lambda_j} \tag{5}$$

Since the variance measures the importance of each eigenvector, it can be used as a criterion for accepting or rejecting an eigenvector. In the case of Si LVV spectra, the sum of top two variances was 0.997 and the variance for the third factor was only 0.0017, which suggests that almost all (99.7 %) of the data set shown in Fig. 5 (c) can be explained by the top two factors. Thus the relative concentration profile shown in Fig. 6 was deduced by the TFA using two factors. Obviously the factors #1 and #2 should correspond to the Si LVV spectra of elemental Si and SiO_2, respectively. As shown in Fig. 7, the test vectors #1 and #2 were selected to represent the Si LVV spectra of elemental Si and SiO_2, respectively. The accordance between the test vectors and the predicted vectors were found to be fairly good. In the depth profile shown in Fig. 6, the values for the relative concentration of the two factors correspond to the column factors of the transformed column matrix $\boldsymbol{C}$. It should be noted that a small deviation is observable in the interface region. That is to

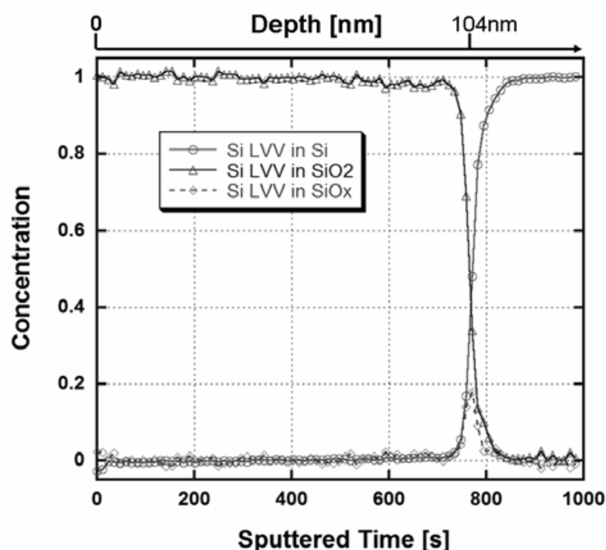

Fig. 6 The depth profile of a SiO_2 thin film (104 nm) on a Si(001) substrate obtained with 1.4 keV Ar^+ beam and an electron beam current density of 0.081 A/cm^2. The profile was obtained by TFA using two factors, where the factor #1 and #2 represent the Si LVV spectra of elemental Si and SiO_2, respectively. Small deviation was observed in the interface region, where the deviation profile was attributed to the SiO_x transition region. The deviation is defined as 1-(C_Si+C_SiO_2) where the C_Si and C_SiO_2 correspond to the concentration of the elemental Si and SiO_2, respectively.

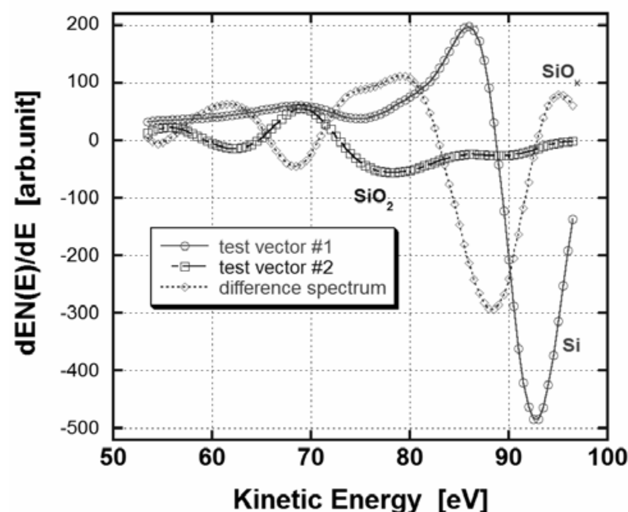

Fig. 7 Test vectors #1 and #2 for Si LVV spectra for elemental Si and SiO_2, respectively, which were employed for the target factor analysis of the depth profiling shown in Fig. 6. The difference spectrum is extracted from the original Auger spectrum at the SiO_2/Si(001) interface where the deviation profile shown in Fig. 6 takes its maximum, which can be attributed to the spectrum of SiO_x.

say, the sum of the two column factors was found to be smaller than unity. The deviation profile is shown by a dashed line in Fig. 6, which has a distinct peak at the SiO_2/Si(001) interface. It has been reported that there exits a transition layer composed of sub-stoichiometric silicon oxide (SiO_x; $1<x<2$) at the SiO_2/Si interface [9,22]. Therefore, it is reasonable to attribute the deviation profile to the relative concentration profile of the SiO_x transition layer composed of oxygen deficient centers. The difference spectrum is extracted from the original Auger spectrum at the SiO_2/Si(001) interface where the deviation profile shown in Fig.6 takes its maximum. Compared with the previous studies on Si LVV spectrum for the SiO_x at the interface between a thermally grown SiO_2 thin film and a Si(001) substrate [17], the peak position (83 eV in *EN(E)* mode and 88 eV in *dEN(E)/dE* mode) of the difference spectrum shows a fairly good agreement. Consequently, it is reasonable to assign this difference spectrum to that originated from the sub-stoichiometric silicon oxide, that is to say, SiO_x. However, it should be noted that previous XPS measurements on the Si 2p spectra at the SiO_2/Si(001) interface demonstrated the existence of three intermediated oxidation states such as Si_2O, SiO and Si_2O_3 [1, 23]. Since AES does not have such a high resolution as XPS, the sub-stoichiometric SiO_x state at the SiO_2/Si(001) interface observed by AES is likely to be a mixture of those intermediate oxidation states. The corresponding O KLL spectra in Fig. 4 (a) indicated the continuous shift to higher kinetic energy, which may also support the presence of the transient sub-stoichiometric oxide at the interface.

4.2 Profile Shift and Depth Resolution

Various information on the property of the SiO_2/Si(001) interface can be extracted from the detailed analysis of the compositional depth profiles. As for the interface width, the difference of the depth coordinate z between 84 and 16 % of the intensity change at the interface gives a measure of the depth resolution Δz in the depth profile [24]. In general, the inelastic mean free path (IMFP) λ affects an observed depth profile in its position and depth resolution. As for the IMFP effects on the depth profiling, a profile shift of approximately 0.7λ with respect to the original depth, and the broadening effect of Δz_λ ($\cong 1.6\lambda$) are expected [25].

Figure 8 shows the comparison of the depth profiles for the SiO_2/Si(001) interface observed with an electron beam current density of 0.081 A/cm^2, which were extracted by TFA. The chemical depth profiles for the SiO_2 state obtained from the three Auger transitions of Si LVV, Si KLL and O KLL, and those of the elemental Si obtained from Si LVV and Si KLL, are shown in Fig. 8 (a) and (b), respectively. In both cases, shift and broadening of the interface profiles were observed.

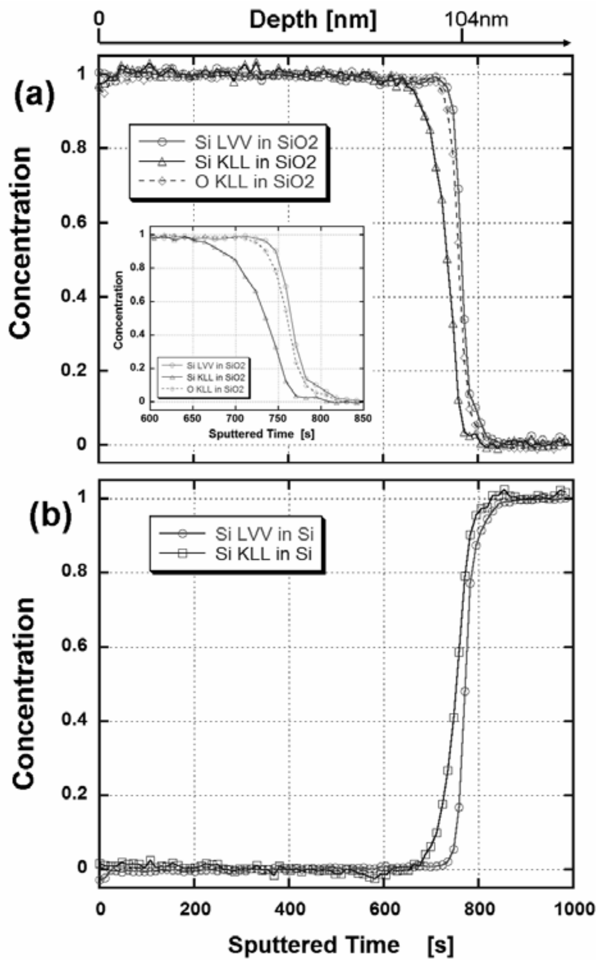

Fig. 8 Comparison of the depth profiles for the SiO_2(104nm)/Si(001) interface with a 1.4 keV Ar^+ beam and an electron beam current density of 0.081 A/cm^2. (a) Chemical depth profiles for the SiO_2 state obtained with Auger transitions of Si LVV, Si KLL and O KLL. (b) Chemical depth profiles for the elemental Si state obtained with Auger transitions of Si LVV and Si KLL.

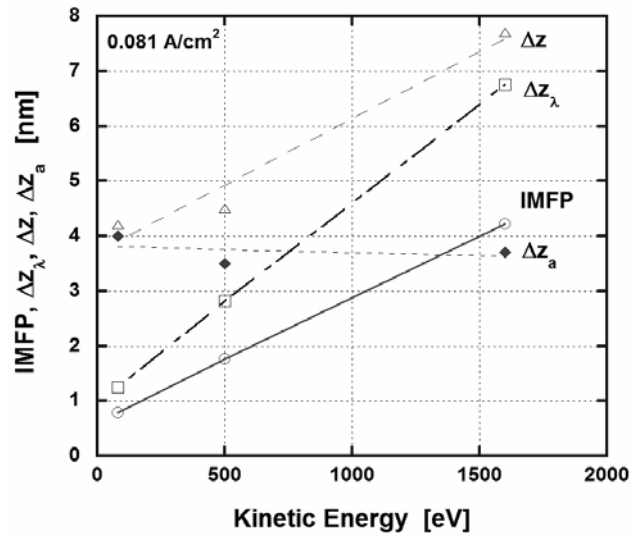

Fig. 9 The depth resolutions Δz are extracted from the TFA depth profiles of the SiO_2(104nm)/Si(001) interface (shown in Fig. 8) with different kinetic energies. The IMFP in SiO_2 and the IMFP broadening effect Δz_λ are indicated for the comparison. The actual interface widths Δz_a obtained by Eq. (6) show almost independent of the kinetic energy as expected.

The IMFPs for the above Auger spectra in SiO_2 were calculated as 0.8, 1.8, and 4.2 nm for the electrons in SiO_2 with kinetic energies of ~80, ~500 and ~1600 eV, respectively [26]. Consequently, the estimated profile shifts are 0.5, 1.2 and 3 nm for the SiO_2 depth profiles extracted from the Si LVV, O KLL and Si KLL spectra, respectively. The observed profile shift between the SiO_2 profiles extracted from Si LVV and O KLL was 0.5 nm, which shows a good agreement with the difference (~0.7 nm) of the predicted profile shifts of the Si LVV and O KLL cases. The observed profile shifts between the SiO_2 and the elemental Si profiles, extracted from Si LVV and Si KLL, were 3.2 nm and 2.5 nm, respectively. These values show fairly good agreements with the difference (2.5 nm) of the estimated profile shifts of the Si LVV and O KLL cases.

It is also possible to extract the depth resolutions of the SiO_2/Si(001) interface from the depth profiles shown in Fig. 8. The total depth resolution, Δz, can be described by the intrinsic interface roughness Δz_i, the IMFP broadening effect Δz_λ, the sputtering-induced roughness Δz_s, atomic mixing effect Δz_k, and so on, as below.

$$\Delta z = \sqrt{\Delta z_i^2 + \Delta z_\lambda^2 + \Delta z_s^2 + \Delta z_k^2 + \cdots} \\ = \sqrt{\Delta z_\lambda^2 + \Delta z_a^2} \tag{6}$$

Here, to make a discussion simple, the original interface roughness and radiation-induced effects are considered as a single parameter of the actual interface width Δz_a.

The observed depth resolutions Δz from the TFA depth profiles (shown in Fig. 8) of the SiO_2(104nm)/Si(001) interface are plotted in Fig. 9 as a function of the kinetic energies. The calculated values of IMFP for the corresponding kinetic energies in SiO_2 [26], the IMFP broadening widths Δz_λ (=1.6λ), and the actual interface widths Δz_a deduced using Eq. (6) are also plotted for the comparison. The deterioration of the depth resolution Δz (4.2 to 7.7 nm) with the increase of kinetic energy was clearly observed. Since the deduced values (3.5-4.0 nm) for the actual interface width Δz_a were found to be almost constant (ave. 3.8 nm), the observed deterioration in Δz can be attributed to the enhancement of IMFP broadening effect with the increase of kinetic energy. The

observed depth resolution Δz observed with Si LVV results to be ~4 nm, which is in keeping with the previously reported interface widths (~3 nm) measured in AES depth profiling with lower current density [17].

4.3 Electron Beam Effects on Depth Profiling

As shown in the previous discussion, at the lowest current density, the electron beam effect on the interface width was negligibly small (<~1 nm). However, the increased current density of primary electron beam was found to have a significant effect on the chemical state profiles.

Figure 10 shows the comparison of the TFA depth profiles for the SiO_2/Si interface obtained with various electron beam current densities from 0.081 to 4.7 A/cm^2. From all of the TFA chemical depth profiles obtained with the Auger transitions of (a) Si LVV, (b) O KLL, and (c) Si KLL, it was found that the increase of electron current density tends to deteriorate the depth resolution and enhance the sputtering rate of SiO_2. With the medium current density of 0.52 A/cm^2, the sputtering time required to reach the interface was decreased about 12 %., which means the enhancement of 12 % in sputtering rate. Further increase of the current density enhanced the sputtering rate, but also it started to exhibit the continuous decrease of the SiO_2 state at the topmost surface region. The latter suggests a considerable amount of oxygen desorption from the topmost SiO_2 region.

Figure 11 indicates the dependence of the apparent sputtering rate (a) and the depth resolution (b) on the electron beam current density, evaluated in the most surface-sensitive case using Si LVV spectra. With the increase of electron current density, the apparent sputtering rate was found to increase monotonously up to twice of the lowest case. The depth resolution was found to be significantly deteriorated with the increase of electron current density. It reached up to 20 times as much as the lowest case. These results suggest that significant errors may occur in the evaluation of thickness and interface width of SiO_2 thin film if the primary electron beam is point-focused or is not raster-scanned in a sufficiently large area during the depth profiling.

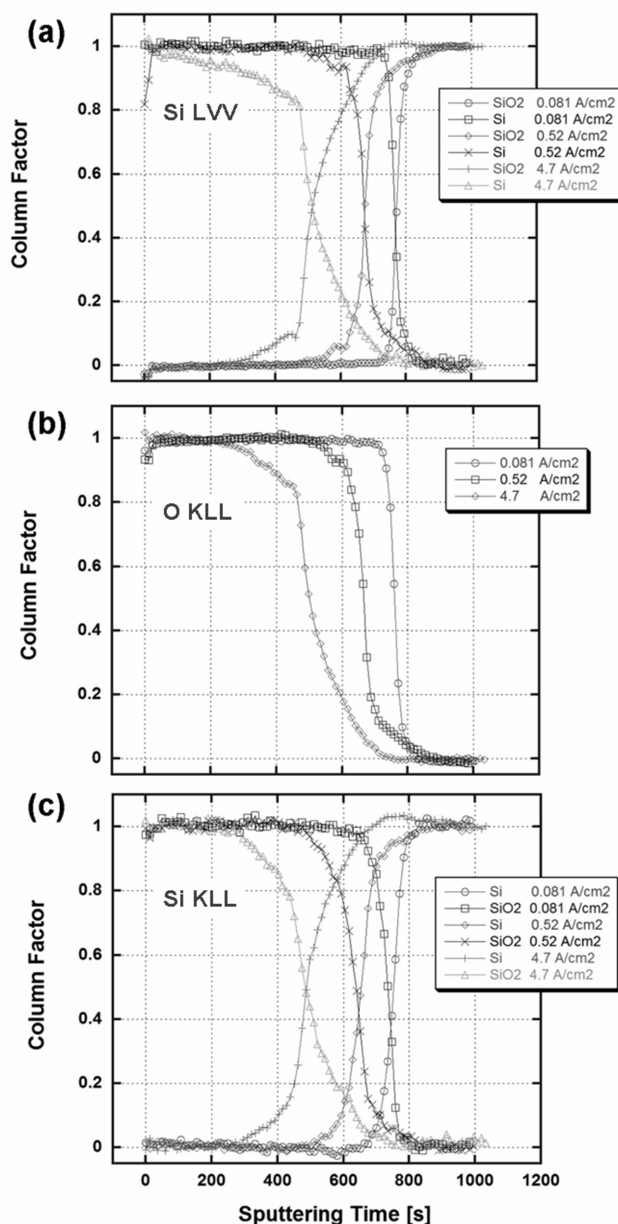

Fig. 10 Comparison of the TFA depth profiles for the SiO_2(104nm)/Si(001) interface obtained with various electron beam current densities. The TFA chemical depth profiles for the elemental Si and SiO_2 states were obtained with Auger transitions of (a) Si LVV, (b) O KLL, and (c) Si KLL.

4.4 Model

Figure 12 shows the proposed model of electron-beam enhanced sputtering of SiO_2 under the irradiation of Ar^+ ion beam. It is well known that SiO_2 decomposes under prolonged electron irradiation [22], which is schematically shown in Fig. 12 (a). Irradiation of sufficiently energetic electrons on the SiO_2 thin film may break the Si-O bonding, and create the dangling bonds and ODC defects [9]. If the electron-induced breaking of bonds occurs at the surface, the created oxygen atoms may come across and be able to desorb as O_2 molecules, which results in the loss of oxygen content at the surface. At room temperature, desorption of SiO is unlikely to occur due to the negligibly small vapor pressure. However, the free oxygen atoms created in relatively deep layer are more likely to be re-trapped by the Si dangling bonds at the ODC defects. Thus the ODC defects created in the deep layer are more likely to be fixed. Therefore, the sub-stoichiometric silicon oxide SiO_x (x<2) composed of the ODC defects is located mostly at the top-most surface region.

When Ar^+ ion beam is irradiated on the SiO_2 involving the decomposed SiO_x on the topmost surface, the sputter-

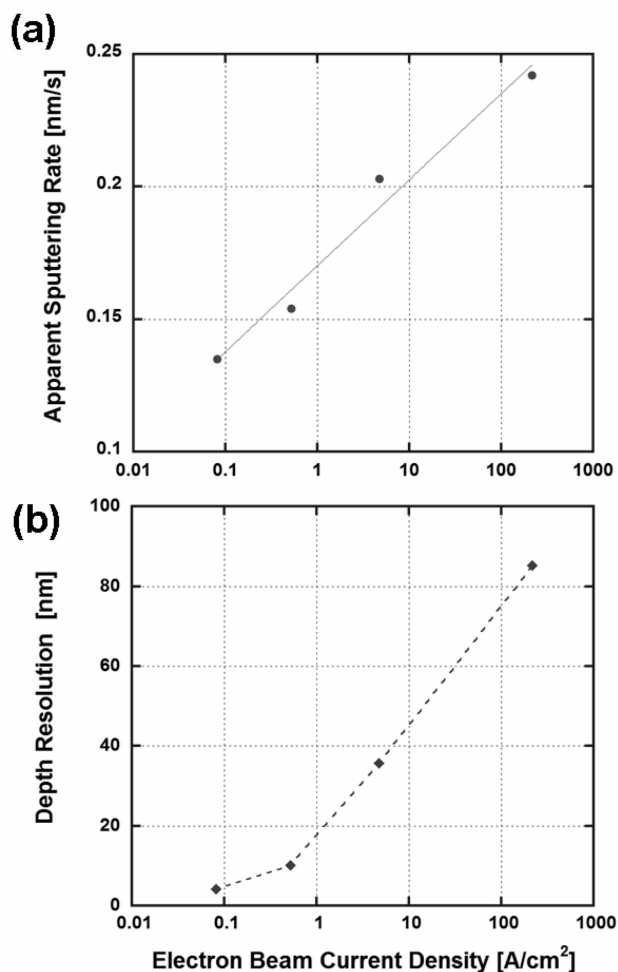

Fig. 11 Dependence of the apparent sputtering rate (a) and the depth resolution (b) on the electron beam current density.

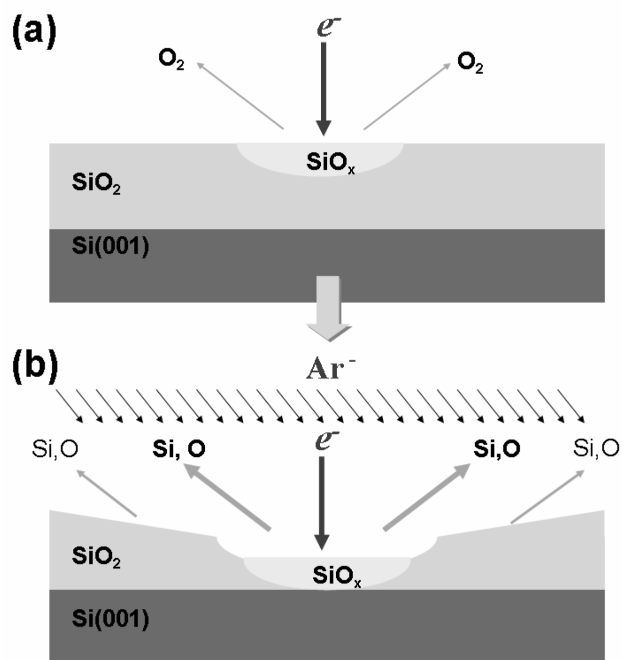

Fig. 12 The proposed model of electron-beam enhanced sputtering of SiO_2 under irradiation of Ar^+ ions.
(a) Electron beam stimulates desorption of oxygen and creates the sub-stoichiometric silicon oxides SiO_x involving the oxygen deficiency centers in the topmost SiO_2 region. (b) The simultaneous irradiation of Ar^+ beam and electron beam causes enhanced sputtering of the electron-beam irradiated area composed of the SiO_x.

ing rate of the SiO_x area should be greater than that of the unperturbed SiO_2 area as schematically shown in Fig. 12 (b). This enhanced sputtering on SiO_x is reasonable because the SiO_x region has very high concentration of ODC defects which are less stable and more likely to be sputtered away than the stoichiometric SiO_2. The enhancement of sputtering rate and subsequent creation of the depression at electron-irradiated region was first demonstrated by Ahn et al [13]. The depth resolution is deteriorated due to the inhomogeneous distribution of ODC defects in the beam-radiated area and the spatial fluctuation of beam-irradiated area.

In order to support the proposed model of enhanced sputtering at the oxygen-deficiency defects, more direct evidence on topography imaging will be required. Now we are planning to perform quantitative AFM measurements at the electron-irradiated area in the sputter-etched crater.

As for the positive application in nanotechnology, the observed enhanced sputtering erosion at the electron-beam irradiated area may be useful for novel nanometer-scale selective etching. Since the increase of the temperature enhance the direct evaporation of SiO, in-situ measurements at the elevated temperatures may give important information for the optimization of the selective etching performance. Theoretical study on the mechanism of ion-beam enhanced sputtering is also required for further progress.

5. Conclusion

Electron beam irradiation effects on the Auger depth profiling with Ar^+ ion-beam sputtering on a SiO_2 thin film formed on Si(001) has been studied using the TFA program. Compared with the conventional peak intensity measurements, the TFA-based depth profiling is more reliable in concentration and more informative as for the number of chemical species involved. Especially the TFA depth profiling has proved itself a powerful tool for chemical state analysis of overlapped Auger peaks originated from SiO_2 and elemental Si. Especially, the existence of sub-stoichiometric oxide with ODC defects at the SiO_2/Si(001) interface has been clarified.

Significant influence of electron beam irradiation on depth profiling has been demonstrated at the beam densities in excess of ~0.5 A/cm^2. Further increase of the electron beam density up to ~200 A/cm^2 lead to the enhancement of the sputtering rate up to ~100 % and the deterioration of the depth resolution up to ~20 times. The observed enhancement in the sputtering rate is attributed to the electron-beam induced desorption of oxygen from the topmost surface region of SiO_2, which creates the less stable sub-stoichiometric SiO_x layer containing ODC defects. Since the SiO_2 thin films on Si(001) substrates are widely used for the calibration of depth scale, careful optimization of beam density using appropriate raster-scanned area is necessary for quantitative evaluation of sputtering rate and depth resolution.

Since the observed enhanced sputtering erosion at the electron-beam irradiated area may be useful for novel nanometer-scale selective etching, theoretical study on the mechanism is required for further progress.

References

[1] S. M. Sze, *Semiconductor Devices, Physics and Technology* , Wiley, (2001) p. 369
[2] M. P. Seah, *Surf. Interf. Anal*., **37**, 300 (2005).
[3] P. A. King, *Surf. Interf. Anal*., **30**, 377 (2000).
[4] S. Hofmann, *Rep. Prog. Phys*. **61**, 827 (1998).
[5] S. Thomas, *J. Appl. Phys*., **45**, 161 (1974).
[6] C. G. Pantano and T. E. Madey, *Appl. Surf. Sci*. **7**, 115 (1981).
[7] P. E. Allen, D. P. Griffis Z. J. Radzimski and P. E. Russell, *J. Vac. Sci. Technol. A*, **10**, 965 (1992).
[8] H. Iwasaki, T. Yoshinobu and K. Sudoh, *Nanotechnology* **14**, R55 (2003).
[9] H. Nonaka, S. Ichimura, K. Arai and C. Le. Greessus, *Surf. Interf. Anal.*, **16**, 435 (1990).
[10] T. Yakabe. D. Fujita and K. Yoshihara, *Appl. Surf. Sci.*, **241**, 127 (2005).
[11] S. Tanuma, T. Kimura, K. Nishida, S. Hashimoto, M. Inoue, T. Ogiwara, M. Suzuki and K. Miura, *Appl. Surf. Sci.* **241**, 122 (2005).
[12] I. Kojima, N. Fukumoto, M. Kurahashi and T. Kameyama, *J. Electron Spectrosc. Relat. Phenom.*, **50**, 53 (1990).
[13] J. Ahn, C. R. Perleberg, D. L. Wilcox, J. W. Coburn and H. F. Winters, *J. Appl. Phys*. **46**, 4581 (1975).
[14] D. Fujita and K. Yoshihara, *J. Surf. Sci. Soc. Jpn.,* **13**, 286 (1992). (in Japanese)
[15] D. Fujita and K .Yoshihara, *J. Surf. Sci. Soc. Jpn*., **14**, 324 (1993). (in Japanese)
[16] K. Yoshihara, D. W. Moon, D. Fujita, K. J. Kim and K. Kajiwara, *Surf. Interf. Anal.*, **20**, 1061 (1993).
[17] M. Sarkar, L. Calliari, L. Gonzo and F. Marchetti, *Surf. Interf. Anal.*, **20**, 60 (1993).
[18] E. R. Malinowski, *Factor Analysis in Chemistry*, 3rd ed., John Wiley & Sons, New York, 2002.
[19] A. Savitzky and M. J. E. Golay, *Anal. Chem*., **36**, 1627 (1964).
[20] W. H. Press, B. P. Flannery, S. Teukolski and W. T. Vetterling, *Numerical Recipes: The Art of Scientific Computing* , Cambridge University Press, Cambridge, 1986.
[21] L. Calliari and F. Marchetti, *Appl. Surf. Sci*., **59**, 79 (1992).
[22] J. S. Johannessen, W. E. Spicer and Y. E. Strausser, *J. Appl. Phys.,* **47**, 3028 (1976).
[23] M. Miyamoto, H. Katakura, Y. Takeda, Y. Takakuwa, N. Miyamoto, A. Hiraiwa and K. Yagi, *J. Vac. Sci. Technol. A*, **9**, 195 (1991).
[24] G. H. Morrison, K. C. Cheng and M. Grasserbauer, *Pure and Appl. Chem*., **51**, 2243 (1979).
[25] S. Hoffmann, *Practical Surface Analysis (Second edition) Vol1: Auger and X-ray Photoelectron Spectroscopy* , ed. by D. Briggs and M. P. Seah, p155. Wiley, Chichester (1990).
[26] S. Tanuma, C. J. Powell and D. R. Penn, *Surf. Interf.Anal*., **17**, 927 (1991).